PERGAMON

International Journal of Heat and Mass Transfer 45 (2002) 1879–1887

International Journal of HEAT and MASS TRANSFER

www.elsevier.com/locate/ijhmt

Effects of radius and heat transfer on the profile of evaporating thin liquid film and meniscus in capillary tubes

Wei Qu [a], Tongze Ma [a,*], Jianyin Miao [b], Jinliang Wang [a]

[a] *Institute of Engineering Thermophysics, Chinese Academy of Sciences, Beijing 100080, People's Republic of China*

[b] *Institute of Spacecraft System Engineering, Chinese Academy of Space Technology, Beijing 100086, People's Republic of China*

Received 2 August 2001

Abstract

The physical and mathematical models are established to account for the formation of evaporating thin liquid film and meniscus in capillary tubes. The core vapor flow is due to gradient of vapor pressure, which is mainly contributed by the shear stress at vapor–liquid interface. The liquid film flow is owing to gradients of capillary pressure and disjoining pressure. The heat transfer is composed of liquid film conduction and evaporation at vapor–liquid interface. The mass balance of vapor flow is considered to obtain the vapor velocity, this can evade directly solving the rarefied gas velocity field.

In regard to the capillary tubes of micron scale, the calculation results show that, the bigger the inner radius or the smaller the heat flow, the longer the evaporating interfacial region will be. There only exists meniscus near the wall, and nearby the axial center is flat interface. While as to the capillary tubes of scale about 100 μm, the evaporating interfacial region will increase with heat flux. Compared with capillaries of micron scale, the meniscus region will extend to the center of capillary axis. These can be tentatively explained as strong influence of the thin liquid film.

For the capillary tubes of radius about 100 μm, the experimental results indicate that the apparent contact angles and meniscus profiles can almost coincide with those of the theoretical values.

Keywords: Capillary tubes; Micron scale; Evaporating thin liquid film; Meniscus

1. Introduction

The radii of capillary tubes used in micro and high efficiency evaporators, such as micro heat pipes and pulsating heat pipes etc., are presently considered from several microns to hundreds of microns. The flow and heat transfer in capillary tubes are still not known thoroughly. As to their mechanisms, investigations on the profiles of thin film and meniscus are very important.

When a heated plate is rewetted by a liquid, the liquid will be adsorbed along the surface forward [1,2]. The wall temperature of falling liquid film has related closely with the heat flux [3]. If the groove structure is used, the thin liquid film and meniscus will form on the groove wall [4–7], and can be divided into three sub-regions [7–10]: equilibrium thin film region, evaporation liquid film region and meniscus region. The disjoining pressure and capillary pressure are the only operational force in the equilibrium thin film region and meniscus region respectively; while in the evaporation liquid film region, the disjoining pressure and capillary pressure exert influences on vapor–liquid interface simultaneously.

Wayner and his co-workers [11–15] had done many researches on thin liquid films, N–S momentum equation is proved to hold true well [16]. However, for vapor flow, if the diameter of flow passage is so small that Knudsen number is greater than 0.001, rarefied gas effect should be considered.

In this paper, the profiles of vapor–liquid interface in the capillary tubes of both micron scale and scale about 100 μm are further investigated to consider the flow and

* Corresponding author. Tel.: +86-10-6255-4189; fax: +86-10-6257-5913.

E-mail address: tzma@public.east.net.cn (T. Ma).

0017-9310/02/$ - see front matter
PII: S0017-9310(01)00296-4

Nomenclature

c_p	specific heat at constant pressure, J/(kg K)
Gr	Grashof number
h_{fg}	latent heat of evaporation, J/kg
k	thermal conductivity, W/(m K)
K	curvature of the surface, m^{-1}
L	length, m
m	mass flow rate, kg/s
Nu	Nusselt number
P	pressure, N/m^2
Pr	Prandtl number
q	heat flux, W/m^2
Q	heat flow, W
r	radius, m
R	universal gas constant, J/(mol K)
R_g	gas constant, J/(kg K)
T	temperature, K
u	velocity, m/s
x	axial coordinate, m

Greek symbols

α	heat transfer coefficient, $W/(m^2\ K)$
δ	thickness of the film, m
ρ	density, kg/m^3
μ	dynamic viscosity, kg/(m s)
ε	emissivity
σ	surface tension, N/m
τ	shear stress, N/m^2

Superscript

$'$	derivative

Subscripts

c	coming liquid
con	convection
f	friction
l	liquid
m	mean
mt	momentum transfer
i	inner
o	outer
r	radial direction
rad	radiation
tot	total
x	axial direction
v	vapor
w	wall
wf	working fluid
δ	surface of liquid film
∞	ambience

evaporation heat transfer characteristics. The vapor velocities are obtained by the handling of mass balance, which can evade the possible difficulty of directly solving the velocity field of non-continuum vapor flow. On the basis of involving the effects of surface forces, some aspects worth attention are as follows: (1) The evaporating interface is not subjectively divided into several sub-regions. The meniscus profile is obtained by non-linear differential equations instead of a global surface approach. (2) The shear stress effects are considered, including one portion due to the momentum transfer of evaporation and the other portion owing to difference of vapor and liquid velocities. (3) The influences of axial pressure gradient of both vapor and liquid film on thickness solution of liquid film are included. The vapor flow gradient is affected by shear stress. (4) The effects of temperature gradient of vapor–liquid interface on the profile of vapor–liquid interface are considered. (5) The wall temperature variations of the capillary tube are calculated simultaneously.

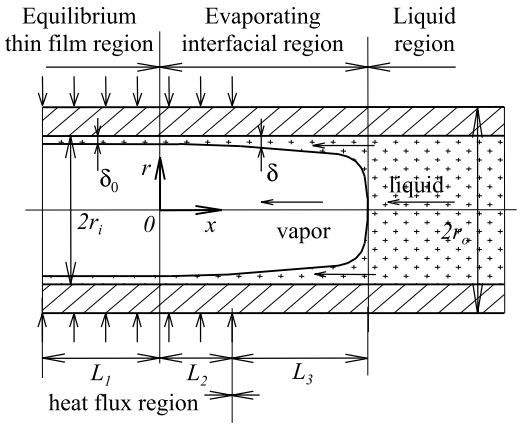

Fig. 1. Illustration of cylidrical coordinate of steady vapor–liquid interface in a capillary tube.

2. Theoretical analysis

As shown in Fig. 1, the following phenomena of heat transfer and flow were analyzed. The heat applied to the capillary wall transfers along the axial capillary wall; part of it conducts through liquid film to vapor–liquid interface and the liquid there evaporates continuously; and the other part conducts forward along capillary wall. The flows of vapor and liquid are driven by the respective pressure gradient, and there exists shear stress between the vapor and liquid. The two vicinity regions

of evaporating interfacial region are equilibrium thin film region and liquid region, respectively. The intersection of the capillary axis and the interface between the equilibrium thin film region and evaporating interfacial region is taken as origin.

Obviously, the applied heat flux and its axial heat transfer determines the highest temperature of the wall. Under a constant liquid supplying pressure, the possible thinnest thickness of adsorbed layer depends on the highest temperature, which can predict the operational limit. In the following analysis, the heat flux is lower than the limit value of combination of the working fluid and capillary tube.

The basic assumptions are as follows: (1) The capillary wall is smooth, the liquid wet the wall completely. (2) The capillary tube operates steadily. (3) Either for liquid film or for vapor, there is no pressure gradient in the radial direction.

2.1. Governing equations of wall temperature

The thickness of capillary tube wall is small, such that the capillary tube wall temperature can be described as

$$\frac{d^2T_w}{dx^2}+\frac{Q_w}{k_w}=0 \tag{1}$$

here, Q_w is mainly due to the thickness variation of the liquid film:

$$Q_w=\frac{2r_o q_w}{r_o^2-r_i^2}-\frac{2k_l(T_w-T_\delta)}{(r_o^2-r_i^2)\ln[r_i/(r_i-\delta)]} \quad (\text{for } 0<x\leqslant L_2), \tag{2}$$

$$Q_w-\frac{2k_l(T_w-T_\delta)}{(r_o^2-r_i^2)\ln[r_i/(r_i-\delta)]} \quad (\text{for } x>L_2). \tag{3}$$

The corresponding boundary conditions can be expressed as

$$\frac{dT_w}{dx}=-\frac{2r_oL_1q_w}{k_w(r_o^2-r_i^2)} \quad (\text{for } x=0), \tag{4}$$

$$\frac{dT_w}{dx}=-\frac{mc_p(T_v-T_c)}{\pi k_w(r_o^2-r_i^2)} \quad (\text{for } x=L_2+L_3). \tag{5}$$

2.2. Temperature of vapor–liquid interface

The evaporation of the vapor–liquid interface depends on both the temperature difference and the pressure difference of the interface to vapor. The local evaporation mass rate of the vapor–liquid interface is given as [6,11,14]

$$\dot{m}_v=a(T_\delta-T_v)+b(P_l-P_v), \tag{6}$$

where

$$a=2\sqrt{\frac{M}{2\pi RT_\delta}}\left(\frac{P_vMh_{fg}}{RT_vT_\delta}\right), \quad b=2\sqrt{\frac{M}{2\pi RT_\delta}}\left(\frac{V_lP_v}{RT_\delta}\right).$$

Considering the geometrical relation, on any cross-section, the evaporation heat transfer per unit length of the capillary tube is obtained as

$$q_\delta=\frac{2\pi(r_i-\delta)}{\cos(\arctan\delta')}[h_{fg}+mc_p(\overline{T}_\delta-T_c)][a(T_\delta-T_v)+b(P_l-P_v)], \tag{7}$$

where $\delta'=d\delta/dx$. The subcooling of the coming liquid is considered together with the latent heat of vaporization.

By Fourier's law, the heat conducted through liquid film for the unit length of axial direction is

$$q_\delta=2\pi r_ik_l\left.\frac{dT}{dr}\right|_{r=r_i}=2\pi k_l(T_w-T_\delta)\Big/\ln\frac{r_i}{r_i-\delta}. \tag{8}$$

Combining Eqs. (7) and (8), the temperature of the vapor–liquid interface will be

$$T_\delta=\frac{T_wk_l/\varepsilon+a_1T_v+b_1\sigma K}{a_1+b_1\rho_lR_g\ln(a\delta^b)+k_l/\varepsilon}, \tag{9}$$

$$\varepsilon=\frac{(r_i-\delta)}{\cos(\arctan(\delta'))}[h_{fg}+mc_p(\overline{T}_\delta-T_c)]\ln\frac{r_i}{r_i-\delta}. \tag{10}$$

2.3. Capillary pressure and disjoining pressure

The capillary pressure can be expressed as

$$P_c=\sigma K, \tag{11}$$

where K represents the twice mean curvature of vapor–liquid interface. It can be given as the sum of circular curvature and axial curvature:

$$K=K_r+K_x. \tag{12}$$

For the circular direction and axial direction, respectively, the surface curvature of liquid film is given, respectively, as

$$K_r=\frac{\cos(\arctan\delta')}{r_i-\delta}=\frac{1}{r_i-\delta}\left[1+\left(\frac{d\delta}{dx}\right)^2\right]^{-1/2}, \tag{13}$$

$$K_x=\frac{d^2\delta}{dx^2}\left[1+\left(\frac{d\delta}{dx}\right)^2\right]^{-3/2}. \tag{14}$$

In this paper, water is taken as working fluid, which is polar strongly. The disjoining pressure, which versus the thickness of the liquid film and the surface temperature, is cited here [8,12]:

$$P_d=\rho_lR_gT_\delta\ln[A\delta^B], \tag{15}$$

where $A=1.49$ and $B=0.0243$.

The pressure difference of vapor and liquid can be given by augmented Young–Laplace equation as

$$P_\mathrm{l} - P_\mathrm{v} = P_\mathrm{d} - \sigma K. \tag{16}$$

2.4. Thickness of liquid film at origin

For equilibrium thin film region ($x \leqslant 0$) there is no evaporation at the film surface, so

$$T_\mathrm{w} = T_\delta, \quad \dot{m}_\mathrm{v} = 0, \quad \delta' \approx 0, \quad \delta'' \approx 0. \tag{17}$$

By Eqs. (12)–(14) and (17), the twice curvature of the vapor–liquid interface at origin is

$$K = 1/(r_\mathrm{i} - \delta_0). \tag{18}$$

The iterative formula of liquid film thickness at origin is obtained by Eqs. (6), (15)–(17) as

$$\delta_0 = \left\{ \frac{1}{A} \exp\left[\frac{1}{b\rho_\mathrm{l} R_\mathrm{g} T_\mathrm{w}} \left(\frac{b\sigma}{r_\mathrm{i} - \delta_0} - a(T_\mathrm{w} - T_\mathrm{v}) \right) \right] \right\}^{1/B}. \tag{19}$$

2.5. Velocities of liquid and vapor

The momentum equation of the liquid film and its corresponding boundary conditions are as follows:

$$\mu_\mathrm{l} \frac{1}{r} \frac{\mathrm{d}}{\mathrm{d}r} \left(r \frac{\mathrm{d}u_\mathrm{l}}{\mathrm{d}r} \right) = \frac{\mathrm{d}P_\mathrm{l}}{\mathrm{d}x}, \tag{20}$$

$$u_\mathrm{l}|_{r=r_\mathrm{i}} = 0, \tag{21}$$

$$\left. \frac{\mathrm{d}u_\mathrm{l}}{\mathrm{d}r} \right|_{r=r_\mathrm{i}-\delta} = \frac{\tau_\delta}{\mu_\mathrm{l}}. \tag{22}$$

Integrating Eq. (20) twice and considering boundary conditions (21) and (22), the velocity of liquid film will be

$$u_\mathrm{l} = \frac{1}{4\mu_\mathrm{l}} \frac{\mathrm{d}P_\mathrm{l}}{\mathrm{d}x} r^2 + c_1 \ln r + c_2. \tag{23}$$

The integral constants are as follows:

$$\begin{aligned} c_1 &= \frac{r_\mathrm{i} - \delta}{\mu_\mathrm{l}} \left(\tau_\delta - \frac{(r_\mathrm{i} - \delta)}{2} \frac{\mathrm{d}P_\mathrm{l}}{\mathrm{d}x} \right), \\ c_2 &= -\frac{r_\mathrm{i}^2}{4\mu_\mathrm{l}} \frac{\mathrm{d}P_\mathrm{l}}{\mathrm{d}x} - c_1 \ln r_\mathrm{i}. \end{aligned} \tag{24}$$

So, the mean velocity of the liquid film is

$$\begin{aligned} u_\mathrm{l,m} &= \frac{1}{\delta} \int_{r_\mathrm{i}-\delta}^{r_\mathrm{i}} u_\mathrm{l} \,\mathrm{d}r \\ &= \frac{1}{12\mu_\mathrm{l}} \frac{\mathrm{d}P_\mathrm{l}}{\mathrm{d}x} (\delta^2 - 3r_\mathrm{i}\delta + 3r_\mathrm{i}^2) + \frac{c_1 r_\mathrm{i}}{\delta} \ln \frac{r_\mathrm{i}}{r_\mathrm{i} - \delta} \\ &\quad + c_1 \ln(r_\mathrm{i} - \delta) - c_1 + c_2. \end{aligned} \tag{25}$$

And the velocity of liquid at vapor–liquid interface can be expressed as

$$u_\mathrm{l}|_{r=r_\mathrm{i}-\delta} = \frac{(r_\mathrm{i} - \delta)^2}{4\mu_\mathrm{l}} \frac{\mathrm{d}P_\mathrm{l}}{\mathrm{d}x} + c_1 \ln(r_\mathrm{i} - \delta) + c_2. \tag{26}$$

For steady state, the total mass flow rate at each cross-section is constant, it consists of the liquid portion and the vapor portion

$$m = m_\mathrm{xl} + m_\mathrm{xv}. \tag{27}$$

So, the mean velocity of vapor at position x and at origin can be given by Eq. (27):

$$u_\mathrm{v,m} = \left(\frac{r_\mathrm{i} - \delta_0}{r_\mathrm{i} - \delta} \right)^2 u_\mathrm{v0,m} + \frac{\rho_\mathrm{l}}{\rho_\mathrm{v}} \left[1 - \left(\frac{r_\mathrm{i} - \delta_0}{r_\mathrm{i} - \delta} \right)^2 \right] u_\mathrm{l,m}, \tag{28}$$

$$u_\mathrm{v0,m} = \frac{2r_\mathrm{o}(L_1 + L_2) q_\mathrm{w}}{(r_\mathrm{i} - \delta_0)^2 \rho_\mathrm{v} h_\mathrm{fg}}. \tag{29}$$

2.6. Axial pressure gradient of vapor flow

The pressure gradient of vapor flow is given as

$$\frac{\mathrm{d}P_\mathrm{v}}{\mathrm{d}x} = -\frac{2\tau_\delta}{r_\mathrm{i} - \delta} - \frac{\mathrm{d}(\rho_\mathrm{v} u_\mathrm{v}^2)}{\mathrm{d}x}. \tag{30}$$

The first term in the right-hand side of Eq. (30) is due to the shear stress between the liquid film and vapor, while the second term is owing to the inertial force of vapor. The shear stress composes the frictional force term, τ_f, induced by the velocity difference of vapor and liquid film, and the shear stress force term τ_mt come from the momentum transfer of evaporation, i.e.,

$$\tau_\delta = \pm(\tau_\mathrm{f} + \tau_\mathrm{mt}). \tag{31}$$

When the mean velocity of vapor is greater than or equal to that of the liquid at the same location, the shear stress is positive or zero, otherwise it is negative. The right two terms of Eq. (31) can be given as follows:

$$\tau_\mathrm{f} = \frac{1}{2} c_\mathrm{f} \rho (u_\mathrm{xv,m} - u_\mathrm{xl}|_{r=r_\mathrm{i}-\delta})^2, \tag{32}$$

$$\tau_\mathrm{mt} = \frac{q_x}{h_\mathrm{fg}} \left| (u_\mathrm{xv,m} - u_\mathrm{xl}|_{r=r_\mathrm{i}-\delta}) \right|. \tag{33}$$

In Eq. (33), q_x is the local heat flux at x. It can be obtained by Fourier's law as

$$q_x = \frac{k_\mathrm{l}(T_\mathrm{w} - T_\delta)}{r_\mathrm{i} \ln[r_\mathrm{i}/(r_\mathrm{i} - \delta)]}. \tag{34}$$

The method of the flow resistance in tube is referenced to calculate the vapor flow resistance relative to static liquid surface.

2.7. Governing equations of liquid film thickness

By Eq. (16), the curvature gradient would be

$$\frac{dK}{dx} = -\frac{1}{\sigma}\left(\frac{dP_l}{dx} - \frac{dP_v}{dx} - \frac{dP_d}{dx}\right). \tag{35}$$

Relate the evaporation heat transfer with the mass flow rate, the pressure gradient of liquid flow is

$$\frac{dP_l}{dx} = \frac{2k_l}{\rho_l h_{fg} c_7}\int_0^x \frac{T_w - T_\delta}{\ln(r_i/(r_i-\delta))}\,dx - \frac{c_8}{c_7}, \tag{36}$$

$$c_4 = \frac{1}{8\mu_l}[r_i^4 - (r_i-\delta)^4], \tag{37}$$

$$c_5 = r_i^2\left(\ln r_i - \frac{1}{2}\right) - (r_i-\delta)^2\left[\ln(r_i-\delta) - \frac{1}{2}\right], \tag{38}$$

$$c_6 = 2r_i\delta - \delta^2, \tag{39}$$

$$c_7 = c_4 - \frac{c_5(r_i-\delta)^2}{2\mu_l} + \frac{c_6}{4\mu_l}(2(r_i-\delta)^2\ln r_i - r_i^2), \tag{40}$$

$$c_8 = (c_5 - c_6\ln r_i)(r_i-\delta)\frac{\tau_\delta}{\mu_l}. \tag{41}$$

The gradient of disjoining pressure can be derived from Eq. (15) as

$$\frac{dP_d}{dx} = \rho_l R_g \ln(A\delta^B)\frac{dT_\delta}{dx} + \frac{B\rho_l R_g T_\delta}{\delta}\frac{d\delta}{dx}. \tag{42}$$

The non-linear differential equation of liquid film thickness is given by Eqs. (12) and (35) as

$$\begin{aligned}&\frac{d^3\delta}{dx^3} - 3\left(\frac{d^2\delta}{dx^2}\right)^2\frac{d\delta}{dx}\left[1+\left(\frac{d\delta}{dx}\right)^2\right]^{-1} \\ &-\frac{d^2\delta}{dx^2}\frac{d\delta}{dx}(r_i-\delta)^{-1} + \frac{d\delta}{dx}\left[1+\left(\frac{d\delta}{dx}\right)^2\right](r_i-\delta)^{-2} \\ &+\frac{1}{\sigma}\left[1+\left(\frac{d\delta}{dx}\right)^2\right]^{1.5}\left[\frac{dP_l}{dx} - \frac{dP_v}{dx} - \frac{dP_d}{dx}\right] = 0.\end{aligned} \tag{43}$$

The differential equations (43), (30), (36) and (42) are numerically solved simultaneously using Runge–Kutta method. For every advanced step, the calculation finishes if the calculated thickness of liquid film is equal to the radius of the capillary tube.

3. Experimental setup

The experimental setup is shown schematically in Fig. 2. The capillary tube is set horizontally. The front end of the capillary tube and the reservoir (not illustrated) are open to the air.

For the sake of eliminating the refraction effect and picture distortion by the wall, the quartz-glass capillary tubes of thin wall are utilized. The inner and outer radii are $r_i = 0.168$ mm, $r_o = 0.312$ mm, respectively.

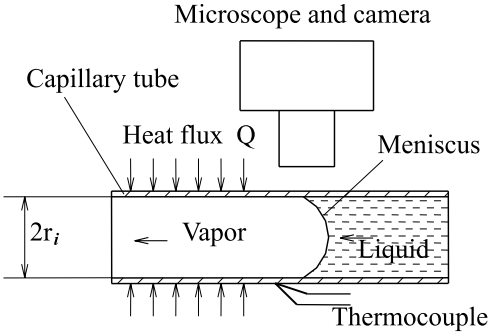

Fig. 2. Schematic of capillary tube setup.

The position of meniscus in the capillary tube can be adjusted by a valve, which controls the height from reservoir liquid surface up to the capillary axis. Since the inner diameter of reservoir, $D = 55$ mm, is much bigger than that of the capillary tube, the vertical distance between the capillary axis and the liquid surface of the reservoir is kept nearly constant during steady operation.

The multi-channel digital thermometer of type WD-10 was used. In order to visualize the meniscus better, only one copper-constantan thermocouple was placed tightly on the wall of the meniscus front. The meniscus was visualized and photographed by a biological microscope, the obtained photographs could be 100 times of the original picture.

After heat is supplied by direct current supply to the capillary wall and the steady state of thermal and fluid flow is obtained, evaporation occurs continuously on the steady vapor–liquid interface and the data can be recorded thereby.

The power is increased step by step from zero. After that, the power is decreased step by step to zero. For every heat flow, when the meniscus is steady, the meniscus profile is photographed by microscope and camera, which can show how the dynamic apparent contact angle changes with heat flow.

4. Calculated and experimental results

The working fluid is distilled water. In order to compare the calculation results with those of experiment, the vapor saturation temperature at tube entrance is set as 373.15 K.

4.1. Numerical results of micron scale capillaries

The typical calculated results of the profile of vapor–liquid interface are summarized in Figs. 3 and 4. The

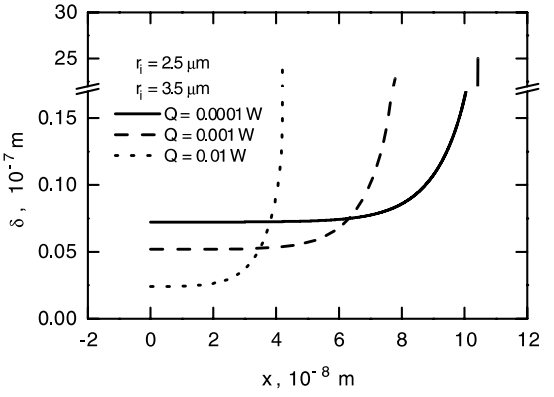

Fig. 3. Effects of heat flow on the profile of vapor–liquid interface in a capillary tube of micron scale.

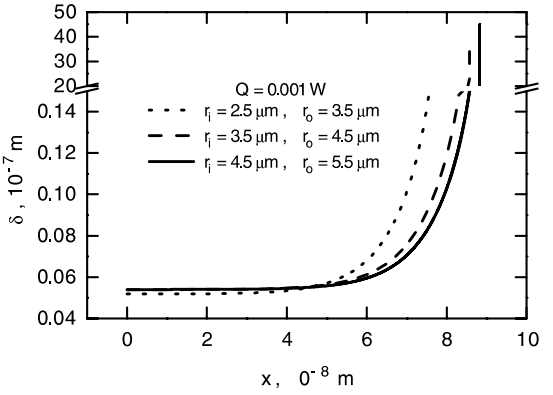

Fig. 4. Influences of capillary radius on the profile of vapor–liquid interface in the capillary tubes of micron scale.

heat flow and radii of capillary tube all exert influences on the profile of vapor–liquid interface in the evaporating interfacial region. As shown from the origin of the evaporating interfacial region, the thickness of liquid film increases gently, about two to three orders smaller than the capillary radius quantitatively, and then increases quickly, especially near the end of evaporating interfacial region. When the thickness of liquid film increases to the value that is one order magnitude smaller than the capillary radius, the thickness of the liquid film gradient is so big that, in the several steps of the following advancing calculation, the calculated thickness of liquid film increases to the capillary radius.

The profiles of vapor–liquid interface have very close relations with the driven forces and interaction between the two sides of the vapor–liquid interface. Obviously, the apparent contact angles of micron scale capillary tubes are nearly all 90°.

For micron scale capillaries, an important conclusion can be drawn out from Figs. 3 and 4 that, the bigger heat flow or the smaller capillary radius, the shorter length of evaporating interfacial region would be. This is different from the situation of conventional macro scale tubes, it can be unified by the heat flux effects to capillary wall. So, for micron scale capillaries, the conclusion is that the length of evaporating interfacial region will be shortened with increasing heat flux. That is, increasing the heat flux will lead to the thinner liquid film, and the mean thermal resistance of thin liquid film becomes smaller.

4.2. Numerical results for capillary tubes of the scale about 100 μm

As illustrated in Fig. 5, for 100 μm scale capillaries, the vapor saturation temperature of thin film front is also set at 373.15 K. Apparently the results coincide with the conventional ideas of small scales. However, the profiles of vapor–liquid interface are different from the situations of micron scale capillaries.

Firstly, the length ratio of the thin liquid film to the evaporation interfacial region decreases greatly. Obviously, the thin liquid film effects are very small for the experimental capillary tube.

Secondly, the profile curve shows that there is a nearly flat increase at the front of the meniscus, this means that there is an apparent contact angle for vapor–liquid interface and capillary wall. The calculated apparent contact angles are about between 30° and 70°. As indicated above, the apparent contact angles of micron scale capillaries are 90°.

Thirdly, with the increase of the heat flow applied to the capillary wall, the length of evaporating interfacial region will increase.

The possible explanation for why the situation of micron scale capillary is different from that of about the scales of 100 μm, is owing to the difference of thin liquid film effects. For the capillary tubes of the scale of about 100 μm, the length ratio of the thin liquid film to the

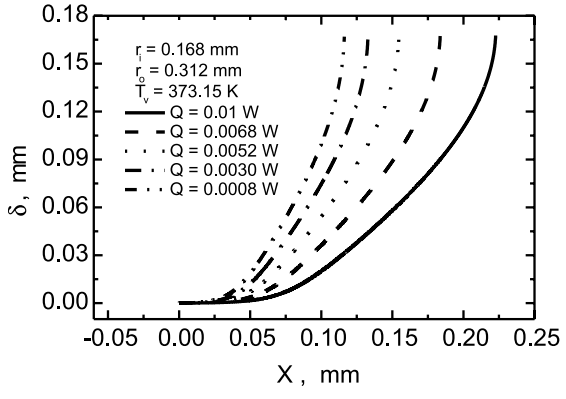

Fig. 5. Profiles of the vapor–liquid interface for different heat flows in a capillary tube of the scale of about 100 μm.

evaporation interfacial region is so small that the effects of thin liquid film is not significant.

4.3. Experimental results

The heat losses from the capillary tube wall due to convection and radiation will be, respectively, as

$$Q_{\mathrm{con}} = 2\pi r_{\mathrm{o}} l_{\mathrm{cool}} h_{\mathrm{con}} (T_{\mathrm{w}} - T_{\infty}), \tag{44}$$

$$Q_{\mathrm{rad}} = 2\pi r_{\mathrm{o}} l_{\mathrm{cool}} \varepsilon \sigma_{\mathrm{rad}} (T_{\mathrm{w}}^4 - T_{\infty}^4), \tag{45}$$

where l_{cool} is the capillary tube length exposed to the ambience, $l_{\mathrm{cool}} = 15$ mm; h_{con} is the convective heat transfer coefficient on outer surface; σ_{rad} is Stefan–Boltzmann constant; ε is the emissivity of capillary wall, $\varepsilon = 0.94$; T_{∞} is the temperature of ambience, $T_{\infty} = 303.15$ K.

At steady evaporation, the force balance can be expressed as

$$(P_{\mathrm{l}} - P_{\mathrm{v}})\pi r_{\mathrm{i}}^2 + 2\pi r_{\mathrm{i}} \sigma \cos\theta - \Delta P_{\mathrm{flow}} \pi r_{\mathrm{i}}^2 = 0, \tag{46}$$

the pressure difference between two sides of the vapor–liquid interface is

$$P_{\mathrm{l}} - P_{\mathrm{v}} = -\rho g H \tag{47}$$

here, H is the height from the reservoir surface up to the horizontal capillary tube axis. The pressure difference due to liquid flow can be related with the mean flow velocity,

$$\Delta P_{\mathrm{flow}} = \frac{8\mu L U}{r_{\mathrm{i}}^2}, \tag{48}$$

where L is the capillary tube length, and the average velocity is

$$\overline{U} = \frac{r_{\mathrm{i}}^2}{8\mu L}\left(\frac{2\sigma}{r_{\mathrm{i}}}\cos\theta - \rho g H\right). \tag{49}$$

So, the mass flow rate would be

$$m = \frac{\rho \pi r_{\mathrm{i}}^4}{8\mu L}\left(\frac{2\sigma}{r_{\mathrm{i}}}\cos\theta - \rho g H\right). \tag{50}$$

Then the evaporation heat flow can be calculated as

$$Q = Q_{\mathrm{tot}} - m c_{\mathrm{p}} (T_{\mathrm{v}} - T_{\mathrm{c}}) - Q_{\mathrm{con}} - Q_{\mathrm{rad}}. \tag{51}$$

With the increasing of wall temperature, the heat loss rate to heating power increases. The heat losses, the heat transfer to the working fluid are evaluated as in Tables 1–3. The actual heat flow to the working fluid for each experiment can be compared with those of theoretical predicted values.

Table 1
Heat loss by radiation

T_{v}, K	332.55	345.95	373.15
Q_{tot}, W	0.0955	0.144	0.262
Q_{rad}, W	0.0107	0.0166	0.0309
$Q_{\mathrm{rad}}/Q_{\mathrm{tot}}$, %	11.2	11.5	11.8

Table 2
Heat loss by convection

T_{v}, K	332.55	345.95	373.15
Pr	0.704	0.703	0.700
Gr	4.236	5.586	7.585
Nu	1.259	1.318	1.396
h_{con}, W/(m^2 K)	30.85	32.27	36.11
Q_{con}, W	0.0481	0.0733	0.134
$Q_{\mathrm{con}}/Q_{\mathrm{tot}}$, %	50.4	50.9	51.1

Table 3
Heat transferred to the working fluid

T_{v}, K	332.55	345.95	373.15
Q_e, W	0.0367	0.0541	0.0972
Q_e/Q_{tot}, %	38.4	37.6	37.1

The photographs of 100 times capillary menisci are illustrated in Fig. 6. The heat flow increased for photograph (1) to (5), and decreased for photograph (5) to (9). These photographs tell us clearly that, the meniscus recedes with increasing heatflow. That is, the length of evaporating interfacial region increases with the heat flow. This coincides with predictions in Fig. 5.

4.4. Discussions

The apparent contact angle recedes when the heat flow increases. The advancing and receding angles are illustrated in Fig. 7. The receding angle is obviously smaller than the advancing angle. The theoretical values without considering the hysteresis are also shown in Fig. 7. The deviation of theoretical contact angle from experimental values increases with decreasing heat flow. This may be owing to the real surface condition of the capillary tubes being different from the ideal smooth assumption.

The effects of the heat fluxes on the axial length of evaporating interfacial region are different in micro space and in macro space. This length will shorten with increasing heat flux for micro space and lengthen with increasing heat flux for macro space. The tentative explanation is that the length shortening or lengthening with heat flux may depend on the length ratio of thin liquid film to evaporation interfacial region and the thermal resistance of thin liquid film. For macro space, length ratio of the axial thin liquid film to the evaporating interfacial region is very small, which is almost zero. The thin liquid film effects are not significant. While for micro space, there exists the thinner liquid film in most length of evaporating interfacial region. That is, the above-mentioned length ratio is very big, its value is nearly one. So, the thin liquid film influences are very important. However, for micro space, the thinner liquid film leads to smaller thermal resistance of the liquid film, for which the evaporating length decreases with heat flux.

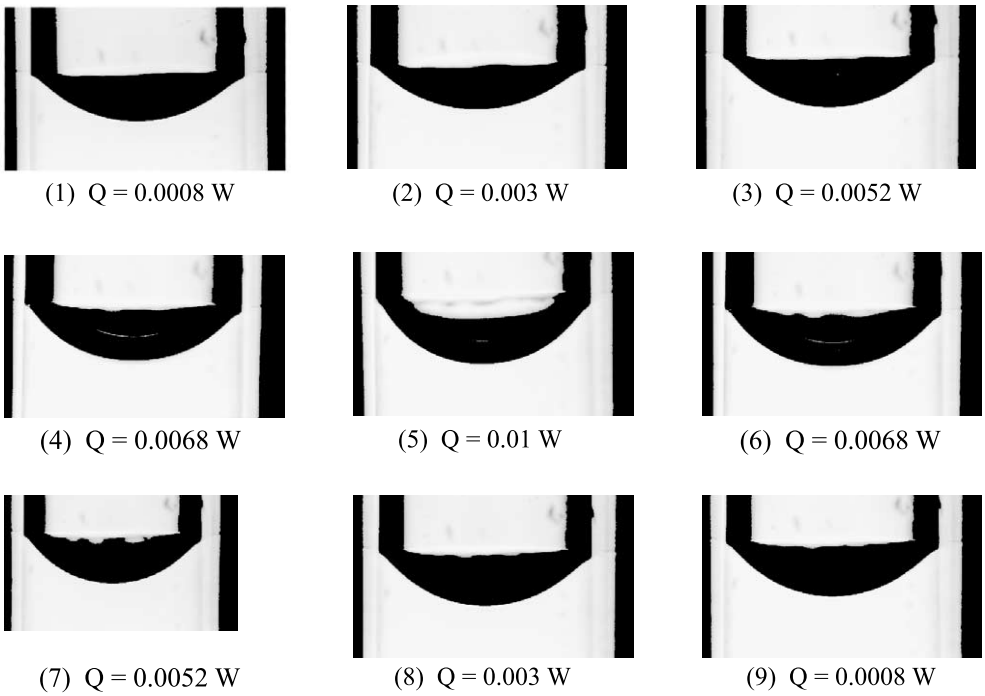

Fig. 6. Photographs of capillary menisci of 100 times, distilled water $r_i = 0.168$ mm, $r_o = 0.312$ mm

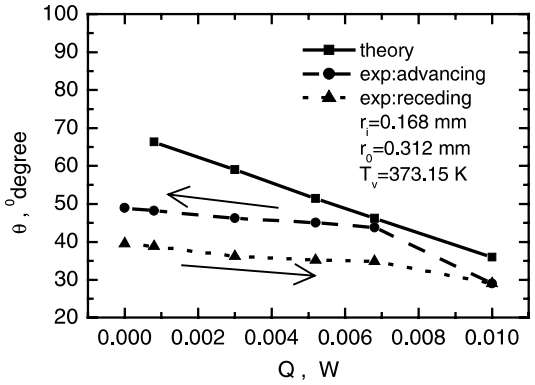

Fig. 7. Comparison of theoretical contact angles with experimental values for a capillary tube of 100 μm radius.

In micro or macro spaces, no matter how the above-mentioned length changes, the local heat transfer coefficients and the temperature of both the capillary tube wall and the vapor–liquid interface all change correspondingly to compensate the decrease or increase of the evaporating length.

5. Conclusions

Two worthwhile attentions can be drawn from the above-mentioned discussions as follows.

For capillary tubes of micron scale, the smaller the heat flux, and/or the bigger the radius of replaced capillary tube, the longer the evaporating interfacial region will be. However, as to capillary tubes of about the scale of 100 μm, the length of evaporating interfacial region will increase with heat flux.

For capillary tubes of micron scale, the meniscus exists only near the wall and nearby the axial center is the flat interface. While for capillary tubes of the scale of about 100 μm, the meniscus region will extend to the center of the capillary axis.

Acknowledgements

This research is financially supported by the National Natural Science Foundation of China with the Grant no. 59995550-4.

References

[1] X.F. Peng, G.P. Peterson, Analysis of rewetting for surface tension induced flow, ASME J. Heat Transfer 114 (1992) 703–707.
[2] D.M. Pratt, K.P. Hallinan, Thermocapillary effects on the wetting characteristics of a heated curved meniscus, J. Thermophys. Heat Transfer 11 (4) (1997) 519–525.

[3] B.X. Wang, J.T. Zhang, X.F. Peng, Experimental study on the dryout heat flux of falling liquid film, Int. J. Heat Mass Transfer 43 (2000) 1897–1903.
[4] H.B. Ma, G.P. Peterson, Temperature variation and heat transfer in triangular grooves with an evaporating film, J. Thermophys. Heat Transfer 11 (1) (1997) 90–97.
[5] X.F. Peng, G.P. Peterson, X.J. Lu, Analysis of capillary-induced rewetting in circular channels with internal grooves, J. Thermophys. Heat Transfer 7 (2) (1993) 334–339.
[6] J.M. Ha, G.P. Peterson, The interline heat transfer of evaporating thin films along a micro grooved surface, ASME J. Heat Transfer 118 (1996) 747–755.
[7] Y. Kobayshi, S. Ikeda, M. Iwasa, Evaporative heat transfer at the evaporative section of a grooved heat pipe, J. Thermophys. Heat Transfer 10 (1) (1996) 83–89.
[8] S.L. Solovy'ev, S.A. Kovalev, Mechanism of Evaporation of a Liquid from a Porous Surface, in: 5th IHPC, Tsukuba Center for Institutes, Japan, 1984, pp. 77–82 (preprints).
[9] J.A. Schonberg, P.C. Wayner Jr., Analytical solution for the integral contact line evaporative heat sink, J. Thermophys. Heat Transfer 6 (1992) 128–134.
[10] K.P. Hallinan, H.C. Chebaro, et al., Evaporation from an extended meniscus for nonisothermal interfacial conditions, J. Thermophys. Heat Transfer 8 (1994) 709–716.
[11] S. DasGupta, J.A. Schonberg, P.C. Wayner Jr., Investigation of an evaporating extended meniscus based on the augmented Young–Laplace equation, ASME J. Heat Transfer 115 (1993) 201–208.
[12] D. Khrustalev, A. Fahgri, Heat transfer during evaporation on capillary-grooved structures of heat pipes, ASME J. Heat Transfer 117 (1995) 740–747.
[13] L.W. Swanson, G.C. Herdt, Model of the evaporating meniscus in a capillary tube, ASME J. Heat Transfer 114 (1992) 434–441.
[14] R. Reyes, P.C. Wayner Jr., A Kelvin–Clapeyron adsorption model for spreading on a heated plate, ASME J. Heat Transfer 118 (1996) 830–882.
[15] D. Khrustalev, A. Faghri, Fluid flow effects in evaporation from liquid–vapor meniscus, ASME J. Heat Transfer 118 (1996) 725–730.
[16] V.P. Carey, Modeling of microscale transport in multiphase systems, in: Proceedings of 11th IHTC, vol. 1, Kyongju, Korea, 1998, pp. 23–40.